A two-fold increase of carbon cycle sensitivity to tropical temperature variations

Article *in* Nature · January 2014

DOI: 10.1038/nature12915 · Source: PubMed

12 authors, including:

Xuhui Wang
Peking University
163 PUBLICATIONS **18,455** CITATIONS
SEE PROFILE

Philippe Ciais
Laboratoire des Sciences du Climat et l'Environnement
1,292 PUBLICATIONS **164,464** CITATIONS
SEE PROFILE

Pierre Friedlingstein
University of Exeter
430 PUBLICATIONS **91,895** CITATIONS
SEE PROFILE

Peter M. Cox
University of Exeter
302 PUBLICATIONS **54,383** CITATIONS
SEE PROFILE

LETTER

doi:10.1038/nature12915

A two-fold increase of carbon cycle sensitivity to tropical temperature variations

Xuhui Wang[1], Shilong Piao[1,2], Philippe Ciais[1,3], Pierre Friedlingstein[4], Ranga B. Myneni[5], Peter Cox[4], Martin Heimann[6], John Miller[7,8], Shushi Peng[1], Tao Wang[1,3], Hui Yang[1] & Anping Chen[9]

Earth system models project that the tropical land carbon sink will decrease in size in response to an increase in warming and drought during this century, probably causing a positive climate feedback[1,2]. But available data[3–5] are too limited at present to test the predicted changes in the tropical carbon balance in response to climate change. Long-term atmospheric carbon dioxide data provide a global record that integrates the interannual variability of the global carbon balance. Multiple lines of evidence[6–8] demonstrate that most of this variability originates in the terrestrial biosphere. In particular, the year-to-year variations in the atmospheric carbon dioxide growth rate (CGR) are thought to be the result of fluctuations in the carbon fluxes of tropical land areas[6,9,10]. Recently, the response of CGR to tropical climate interannual variability was used to put a constraint on the sensitivity of tropical land carbon to climate change[10]. Here we use the long-term CGR record from Mauna Loa and the South Pole to show that the sensitivity of CGR to tropical temperature interannual variability has increased by a factor of 1.9 ± 0.3 in the past five decades. We find that this sensitivity was greater when tropical land regions experienced drier conditions. This suggests that the sensitivity of CGR to interannual temperature variations is regulated by moisture conditions, even though the direct correlation between CGR and tropical precipitation is weak[9]. We also find that present terrestrial carbon cycle models do not capture the observed enhancement in CGR sensitivity in the past five decades. More realistic model predictions of future carbon cycle and climate feedbacks require a better understanding of the processes driving the response of tropical ecosystems to drought and warming.

Climate variability related to El Niño/Southern Oscillation has a dominant role in forcing year-to-year variation in CGR, particularly the forcing of temperature variability[9–13] (Fig. 1a and Extended Data Fig. 1). The observed positive correlation between CGR and temperature reflects the direct impacts of temperature variations in driving variations of tropical carbon fluxes[9,10], rather than, in reverse, the greenhouse effect of atmospheric CO_2 (Methods). Because tropical temperatures are thought to be close to the optimal photosynthetic temperature[14], rising tropical temperatures could decrease vegetation photosynthesis and increase ecosystem respiration, which amplifies the influence of temperature on ecosystem carbon exchange[9]. However, vegetation productivity and respiration both increase with higher precipitation and thus offset each other[9]. These processes lead to a weaker correlation of CGR with precipitation[9] (with coefficient $R = -0.19$; $P > 0.10$) than that of CGR with temperature, on interannual timescale. An application of causality analysis (convergent cross-mapping[15]) also shows that temperature is the major climatic driver of CGR variations (Extended Data Fig. 2). Below, by analysing the atmospheric CO_2 record, we investigated how the sensitivity of tropical carbon fluxes to tropical land surface mean annual temperature (MAT) has changed over the past five decades (Methods).

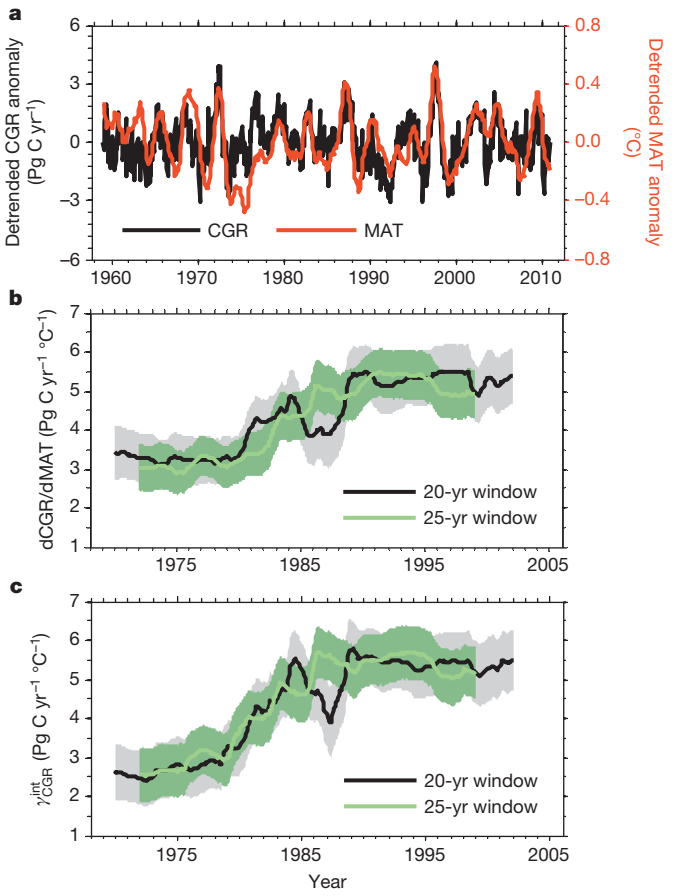

Figure 1 | Change in detrended anomalies in CGR and tropical MAT, in dCGR/dMAT and in γ^{int}_{CGR} over the past five decades. **a**, Change in detrended CGR anomalies at Mauna Loa Observatory (black) and in detrended tropical MAT anomalies (red) derived from the CRU data set[16]. Tropical MAT is calculated as the spatial average over vegetated tropical lands (23° N to 23° S). The highest correlations between detrended CGR and detrended tropical MAT are obtained when no time lags are applied ($R = 0.53$, $P < 0.01$). **b**, Change in dCGR/dMAT during the past five decades. **c**, Change in γ^{int}_{CGR} during the past five decades. In **b** and **c**, different colours show dCGR/dMAT or γ^{int}_{CGR} estimated with moving time windows of different lengths (20 yr and 25 yr). Years on the horizontal axis indicate the central year of the moving time window used to derive dCGR/dMAT or γ^{int}_{CGR} (for example, 1970 represents period 1960–1979 in the 20-yr time window). The shaded areas show the confidence interval of dCGR/dMAT and γ^{int}_{CGR}, as appropriate, derived using 20-yr or 25-yr moving windows in 500 bootstrap estimates.

[1]Sino-French Institute for Earth System Science, College of Urban and Environmental Sciences, Peking University, Beijing 100871, China. [2]Institute of Tibetan Plateau Research, Chinese Academy of Sciences, Beijing 100085, China. [3]Laboratoire des Sciences du Climat et de l'Environnement, CEA CNRS UVSQ, 91191 Gif-sur-Yvette, France. [4]College of Engineering, Mathematics, and Physical Sciences, University of Exeter, Exeter EX4 4QF, UK. [5]Department of Earth and Environment, Boston University, Boston, Massachusetts 02215, USA. [6]Max Planck Institute for Biogeochemistry, 07701 Jena, Germany. [7]Global Monitoring Division, Earth System Research Laboratory, National Oceanic and Atmospheric Administration, 325 Broadway, Boulder, Colorado 80305, USA. [8]Cooperative Institute for Research in Environmental Sciences, University of Colorado, Boulder, Colorado 80309, USA. [9]Department of Ecology and Evolutionary Biology, Princeton University, Princeton, New Jersey 08544-1003, USA.

The linear regression slope between CGR and tropical MAT (dCGR/dMAT) indicates the sensitivity of the tropical carbon cycle to climate interannual variability, and was used to constrain future projections of carbon cycle/climate feedbacks[10]. Using CGR at Mauna Loa Observatory and tropical MAT from the Climatic Research Unit (CRU) at the University of East Anglia[16], we first calculated how dCGR/dMAT changes with time using a 20-yr moving window between 1960 and 2011 (both variables detrended; Fig. 1b). Within each moving window, there is a significant positive correlation between CGR and MAT ($R = 0.49$–0.71, $P < 0.01$). Furthermore, dCGR/dMAT increased from 3.4 ± 0.4 Pg C yr^{-1} °C^{-1} (all uncertainties are s.e.; Pg C, petagrams of carbon) during 1960–1979 to 5.4 ± 0.4 Pg C yr^{-1} °C^{-1} during 1992–2011 (Fig. 1b).

When interpreting this observed long-term increase of dCGR/dMAT, it might be argued that it does not reflect the change in the true response of CGR to temperature variations, but could be due to indirect effects of other climate variables that tend to covary with temperature, such as precipitation and solar radiation. Therefore, to isolate the role of temperature better, we defined the interannual temperature sensitivity of CGR (γ^{int}_{CGR}) as the partial derivative of CGR with respect to MAT in a multiple regression of CGR against MAT, precipitation and solar radiation (all variables detrended; Methods). The increase in dCGR/dMAT was found to reflect mainly an enhanced γ^{int}_{CGR}, rather than a change induced by covariations with the other climate variables (Extended Data Fig. 3). As shown in Fig. 1c, the value of γ^{int}_{CGR} has increased by a factor of two, from 2.7 ± 0.4 Pg C yr^{-1} °C^{-1} to 5.5 ± 0.4 Pg C yr^{-1} °C^{-1} between 1960–1979 and 1992–2011. The window-by-window changes in γ^{int}_{CGR} were fitted with three different models (the Mann–Kendall trend test, a regime shift model and a linear trend model), all of which showed that γ^{int}_{CGR} has increased over the past five decades. However, there are too few degrees of freedom, as a result of data overlapping in neighbouring time windows. Thus, we focus below on the difference in γ^{int}_{CGR} between the earliest time window (the first 20–25 yr) and the most recent time window (the past 20–25 yr), which are derived from fully independent subsets of the data (Methods).

We assessed the robustness of the inferred enhancement in γ^{int}_{CGR} between the first and the last 20–25-yr period of the Mauna Loa CO_2 records. Given the significant disturbance caused by the Mount Pinatubo eruption to the global carbon cycle[17], we first proposed that the cooler post-Pinatubo years characterized by enhanced carbon sinks were an unusual response of carbon sinks to MAT, which could alone explain the higher γ^{int}_{CGR} value of the most recent two decades. Thus, we excluded the two years following the Mount Pinatubo eruption (1992–1993) from our calculation of γ^{int}_{CGR}, which had very little effect on its value, during the most recent two decades (5.4 ± 0.4 Pg C yr^{-1} °C^{-1}) (Extended Data Fig. 4a). To investigate whether extreme years could explain the enhancement in γ^{int}_{CGR}, we performed 500 bootstrap analyses by randomly selecting a subset of data in each 20-yr moving window to calculate γ^{int}_{CGR}. The confidence interval of these estimates is shown in Fig. 1c and confirms that the increase in γ^{int}_{CGR} is not particularly sensitive to a few extreme years. For instance, we still obtain a significant increase in γ^{int}_{CGR} (by a factor of 2.3–2.6) when excluding the two highest positive anomalies in CGR (Fig. 1a), which correspond to the El Niño events of 1972–1973 and 1997–1998, respectively (Extended Data Fig. 4b).

We further verified that the enhancement in γ^{int}_{CGR} over the past five decades is robust with respect to (1) the length of the moving window for calculating γ^{int}_{CGR} (ranging from 20 to 25 yr); (2) the application of a frequency decomposition method by singular spectrum analysis[18] to separate the interannual-timescale component in CGR and MAT, instead of linear detrending (this resulted in γ^{int}_{CGR} increasing by a factor of 1.7 for the 25-yr time windows and by a factor of 2.0 for the 20-yr time windows; Extended Data Fig. 4c); (3) the choice of climate data, using MAT from the Global Historical Climate Network[19], precipitation from Global Precipitation Climatology Centre[20] and data on short-wave radiation[21] (γ^{int}_{CGR} increased by a factor of 1.9–2.1; Extended Data Fig. 4d); and (4) the choice of the other long-term CO_2 record from the South Pole (Methods) instead of Mauna Loa (γ^{int}_{CGR} increased by a factor of 1.7–1.9; Extended Data Fig. 4e). Overall, by analysing the histogram distribution of γ^{int}_{CGR} values obtained with different data sources and different sensitivity tests described above (Methods), we conclude that γ^{int}_{CGR} has robustly increased from 2.6 ± 0.5 Pg C yr^{-1} °C^{-1} to 4.8 ± 1.0 Pg C yr^{-1} °C^{-1} (Fig. 2a). This represents an average relative increase by a factor of 1.9 ± 0.3 (Fig. 2b). This enhancement is very unlikely to have resulted by chance ($<10^{-4}$).

Finally, we applied the same analysis using the land sink calculated as a residual from all other terms of the global carbon budget, as an alternative to CGR for measuring variations in the global land carbon balance[22], and also verified a doubling of $\gamma^{int}_{Land\ Sink}$ (Extended Data Fig. 4f). This test demonstrates that enhanced γ^{int}_{CGR} is not explained by any known change in the variability of fossil fuel fluxes, ocean fluxes or emission from land-use change.

Tropical lands have experienced increasing drought in the past five decades[23,24], particularly from the mid 1970 s to the early 1990 s (Extended Data Fig. 5), when the increase in γ^{int}_{CGR} began (Fig. 1c). On the regional scale, the more recent period (1992–2011) is drier than the earlier period (1960–1979), mainly in northern and central Africa and eastern South America (Extended Data Fig. 6), where a significant correlation between local MAT variability and CGR is observed (Extended Data Fig. 1). Large uncertainties exist in the spatiotemporal patterns of tropical drought changes, as indicated by the spread in the temporal evolution of three drought indices (the annual Palmer drought severity index[23] (PDSI),

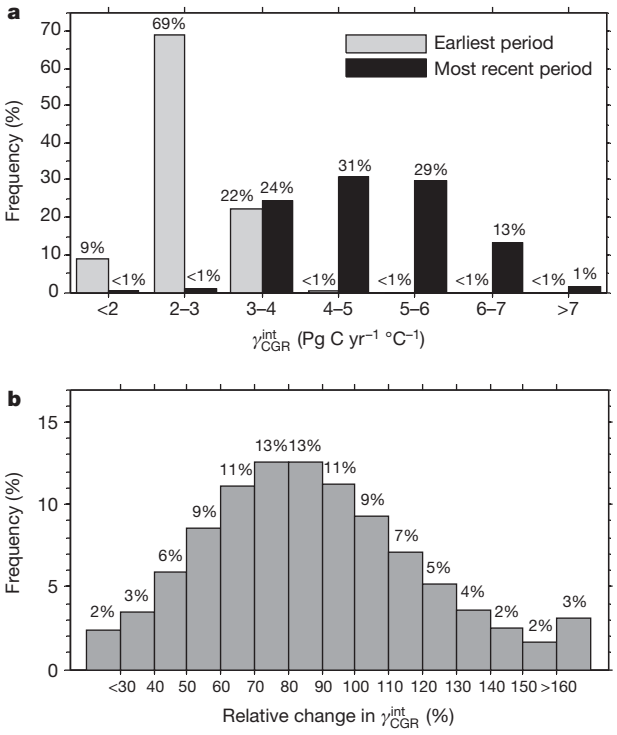

Figure 2 | Histograms of γ^{int}_{CGR} during the earliest period and during the most recent period, and of relative change in γ^{int}_{CGR} over the past five decades. **a**, Early–recent comparison; **b**, relative change. The relative change in γ^{int}_{CGR} is the ratio of the calculated difference in γ^{int}_{CGR} between the most recent period (1992–2011 for a 20-yr time-window) and the earliest period (1960–1979 for 20-yr time window) to the value of γ^{int}_{CGR} during the earliest period. The histograms of γ^{int}_{CGR} and of relative changes in γ^{int}_{CGR} are calculated using bootstrap analyses, considering different data sources (CGR from Mauna Loa or the South Pole, MAT from CRU[16] or the Global the Historical Climate Network[19], precipitation from CRU[16] or the Global Precipitation Climatology Centre[20], and solar radiation from CRU-NCEP, ref. 21 and cloud fraction from CRU[16] as a surrogate), different moving-window lengths (20–25 yr) to calculate the γ^{int}_{CGR}, and different methods to filter out the long-term increase in CGR with time (linear regression and singular spectrum analysis[18]).

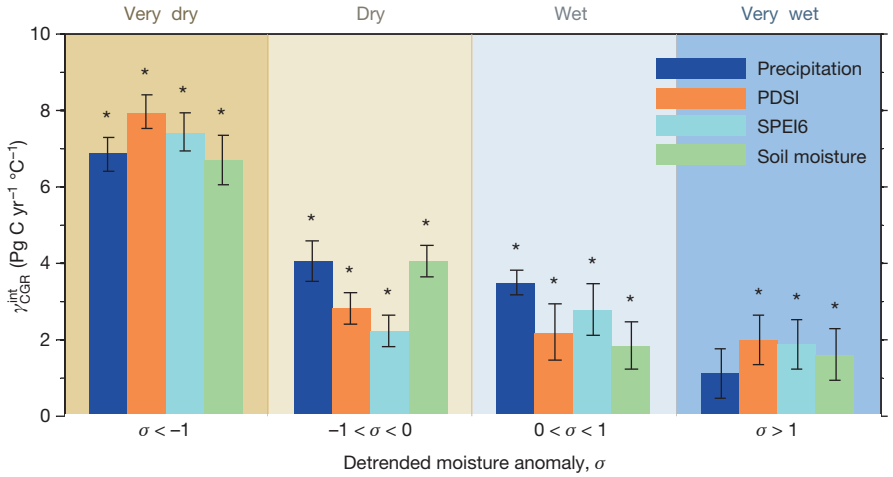

Figure 3 | γ^{int}_{CGR} for each bin of detrended tropical moisture anomaly. Two different drought indicators (PDSI and SPEI calculated on the 6-month scale (SPEI6)), ORCHIDEE-estimated soil moisture and precipitation were used. We grouped the 50 years' worth of data into four distinct bins of detrended tropical moisture anomaly: very dry (σ less than -1), dry (σ between -1 and 0), wet (σ between 0 and 1) and very wet (σ greater than 1) (Methods). We then calculated γ^{int}_{CGR} for each bin of detrended moisture anomaly, using Mauna Loa CO_2 records. The error bars indicate the s.e. of γ^{int}_{CGR} calculated using bootstrap method (Methods). *$P < 0.05$ for γ^{int}_{CGR} being significantly different from zero.

the standardized precipitation–evapotranspiration index[24] (SPEI) and the soil moisture estimated from the ORCHIDEE model[25]; Extended Data Figs 5 and 6). For instance, the ORCHIDEE-estimated soil moisture shows an increase since the 1990s, whereas PDSI and SPEI are comparatively flat during the same period (Extended Data Fig. 5). To gain insight into the possible impact of tropical droughts on γ^{int}_{CGR}, we grouped γ^{int}_{CGR} into different bins of detrended tropical moisture anomaly (Methods). Figure 3 shows that γ^{int}_{CGR} is higher when tropical regions are drier. A Monte Carlo null experiment, assuming no change in moisture conditions, indicates that this relationship between γ^{int}_{CGR} and drought is very unlikely to occur purely by chance ($P < 0.01$; Extended Data Fig. 7). This result suggests that soil moisture may control the response of tropical terrestrial carbon fluxes to temperature fluctuations. Many tropical ecosystems are not only subject to high temperature close to the optimal temperature of photosynthesis[14], but are also subject to water limitations, at least during a dry season. Below a critical threshold for plant root water uptake, soil moisture will limit any temperature-driven increase in evapotranspiration during a warmer year. Photosynthesis will thus drop during a warmer year when soil moisture is limiting during a dry period. In turn, a reduction in photosynthesis will probably result in a larger anomaly of CO_2 input to the atmosphere[26], because respiration usually decreases less than photosynthesis during drought. A soil-moisture-threshold-like response of photosynthesis to temperature interannual anomalies thus can qualitatively explain why γ^{int}_{CGR} is higher during drier periods, but additional investigation is needed to confirm that this is the main mechanism. Droughts in mid latitudes (23°–48° north) have also increased, mostly over the past decade[27] (Extended Data Fig. 5), but this is inconsistent with the observed change in γ^{int}_{CGR} (Fig. 1c). Further statistical analyses suggest that changes in mid-latitude climate must have only minor impacts on the observed γ^{int}_{CGR} change (Extended Data Fig. 8).

Next, we explored whether terrestrial carbon cycle models can capture the observed increase in γ^{int}_{CGR} over the past 50 years. To address this issue, we calculated the temperature sensitivity of simulated tropical net biome productivity ($\gamma^{int}_{mod\ NBP}$) estimated by an ensemble of five terrestrial biosphere models (Methods) previously used in ref. 22 to reconstruct historical changes in the carbon budget. We found that only one model produced an enhancement in $\gamma^{int}_{mod\ NBP}$ over the past five decades, and that enhancement was much smaller in magnitude than the observed change (Extended Data Fig. 9). This implies that most of the models used do not correctly capture the response of tropical carbon fluxes to climate variability[9], probably because of biases in the response of productivity or ecosystem respiration to climate, or because of inaccurate representations of soil temperature and moisture in these models. Thus, the problems present models have in reproducing the observed response of the carbon cycle to climate variability on interannual timescales may call into question their ability to predict the future evolution of the carbon cycle and its feedbacks to climate. Yet it should also be noted that a realistic simulation of the interannual carbon cycle dynamics provides a necessary but not sufficient test of a model's performance for the next century, because, on longer timescales, additional processes such as forest dynamics and changes in soil carbon stocks with low turnover rates become important as well[28].

The terrestrial carbon cycle has experienced significant changes over the past five decades[17,29,30]. In addition to the enhanced magnitude of the land carbon sink[17,29], the observed significant enhancement in γ^{int}_{CGR} found in this study provides a new perspective on a possible shift in the terrestrial carbon cycle. Increased tropical droughts are found to be related to γ^{int}_{CGR} enhancement, highlighting the potentially important role of moisture-temperature interaction in regulating the terrestrial carbon cycle. But it should also be noted that our understanding of the mechanism of γ^{int}_{CGR} enhancement is still limited. Further studies are needed on the response of fundamental carbon cycle processes in the tropical ecosystems and of the sensitivity of ecosystem composition and structure to environmental change. New insights could be obtained from integrated studies, combining dynamic vegetation models with data from long-term manipulative field experiments. Furthermore, new observations of atmospheric CO_2 over tropical land masses from aircraft, towers and satellites may allow for more accurate correlation with climate variables than using Mauna Loa or South Pole CO_2 data.

METHODS SUMMARY

To estimate the interannual sensitivity of CGR to tropical MAT (γ^{int}_{CGR}), we use atmospheric CGR from the two longest atmospheric records at Mauna Loa and South Pole, gridded MAT from the CRU[16] and from Global Historical Climate Network data[19], annual precipitation from CRU and from the Global Precipitation Climatology Centre[20], solar radiation data from CRU-NCEP and ref. 21, and cloud fraction from CRU over vegetated areas (Methods) in the tropics. The value of γ^{int}_{CGR} was calculated as the regression coefficient of temperature in a multilinear regression of CGR variations against variations in temperature, precipitation and solar radiation over a running time window (ranging from 20 to 25 yr). Several statistical tests (Methods) were done to assess the robustness of the increase in γ^{int}_{CGR} over the past five decades. Two different drought indicators (PDSI[23] and SPEI[24]) and soil moisture estimated using the ORCHIDEE model[25] were used to investigate the effects of drought on γ^{int}_{CGR}. We grouped the 50 years of data into four distinct bins of detrended tropical moisture anomaly (standardized departure (σ) less than -1, between -1 and 0, between 0 and 1, and more than 1). For each bin of detrended

moisture anomaly, we calculated γ^{int}_{CGR}. Finally, the outputs of five terrestrial carbon cycle models[22] were analysed to test whether these models could capture the observed increase in γ^{int}_{CGR} during the past 50 years.

Online Content Any additional Methods, Extended Data display items and Source Data are available in the online version of the paper; references unique to these sections appear only in the online paper.

Received 26 July; accepted 27 November 2013.
Published online 26 January 2014.

1. Cox, P. M., Betts, R. A., Jones, C. D., Spall, S. A. & Totterdell, I. J. Acceleration of global warming due to carbon-cycle feedbacks in a coupled climate model. *Nature* **408,** 184–187 (2000).
2. Sitch, S. *et al.* Evaluation of the terrestrial carbon cycle, future plant geography and climate-carbon cycle feedbacks using five dynamic global vegetation models (DGVMs). *Glob. Change Biol.* **14,** 2015–2039 (2008).
3. Phillips, O. L. *et al.* Drought sensitivity of the Amazon rainforest. *Science* **323,** 1344–1347 (2009).
4. Meir, P. & Woodward, F. I. Amazonian rain forests and drought: response and vulnerability. *New Phytol.* **187,** 553–557 (2010).
5. Davidson, E. A. *et al.* The Amazon basin in transition. *Nature* **481,** 321–328 (2012).
6. Baker, D. F. *et al.* TransCom 3 inversion intercomparison: Impact of transport model errors on the interannual variability of regional CO_2 fluxes, 1988–2003. *Glob. Biogeochem. Cycles* **20,** GB1002 (2006).
7. Lee, K., Wanninkhof, R., Takahashi, T., Doney, S. C. & Feely, R. A. Low interannual variability in recent oceanic uptake of atmospheric carbon dioxide. *Nature* **396,** 155–159 (1998).
8. Alden, C. B., Miller, J. B. & White, J. W. C. Can bottom-up ocean CO2 fluxes be reconciled with atmospheric ^{13}C observations? *Tellus B* **62,** 369–388 (2010).
9. Wang, W. *et al.* Variations in atmospheric CO_2 growth rates coupled with tropical temperature. *Proc. Natl Acad. Sci. USA* **110,** 13061–13066 (2013).
10. Cox, P. M. *et al.* Sensitivity of tropical carbon to climate change constrained by carbon dioxide variability. *Nature* **494,** 341–344 (2013).
11. Patra, P. K., Ishizawa, M., Maksyutov, S., Nakazawa, T. & Inoue, G. Role of biomass burning and climate anomalies for land-atmosphere carbon fluxes based on inverse modeling of atmospheric CO_2. *Glob. Biogeochem. Cycles* **19,** GB3005 (2005).
12. Keeling, C. D., Whorf, T. P., Wahlen, M. & van der Plichtt, J. Interannual extremes in the rate of rise of atmospheric carbon dioxide since 1980. *Nature* **375,** 666–670 (1995).
13. Adams, J. M. & Piovesan, G. Long series relationships between global interannual CO2 increment and climate: evidence for stability and change in role of the tropical and boreal-temperate zones. *Chemosphere* **59,** 1595–1612 (2005).
14. Corlett, R. T. Impacts of warming on tropical lowland rainforests. *Trends Ecol. Evol.* **26,** 606–613 (2011).
15. Sugihara, G. *et al.* Detecting causality in complex ecosystems. *Science* **338,** 496–500 (2012).
16. Mitchell, T. D. & Jones, P. D. An improved method of constructing a database of monthly climate observations and associated high-resolution grids. *Int. J. Climatol.* **25,** 693–712 (2005).
17. Sarmiento, J. L. *et al.* Trends and regional distributions of land and ocean carbon sinks. *Biogeosciences* **7,** 2351–2367 (2010).
18. Mahecha, M. D. *et al.* Characterizing ecosystem-atmosphere interactions from short to interannual time scales. *Biogeosciences* **4,** 743–758 (2007).
19. Smith, T. M., Reynolds, R. W., Peterson, T. C. & Lawrimore, J. Improvements to NOAA's historical merged land–ocean surface temperature analysis (1880–2006). *J. Clim.* **21,** 2283–2296 (2008).
20. Schneider, U. *et al.* GPCC's new land surface precipitation climatology based on quality-controlled in situ data and its role in quantifying the global water cycle. *Theor. Appl. Climatol.* http://dx.doi.org/10.1007/s00704-013-0860-x (2013).
21. Sheffield, J., Goteti, G. & Wood, E. F. Development of a 50-year high-resolution global dataset of meteorological forcings for land surface modeling. *J. Clim.* **19,** 3088–3111 (2006).
22. Le Quéré, C. *et al.* Trends in the sources and sinks of carbon dioxide. *Nature Geosci.* **2,** 831–836 (2009).
23. Dai, A. Characteristics and trends in various forms of the Palmer drought severity index during 1900–2008. *J. Geophys. Res.* **116,** D12115 (2011).
24. Vicente-Serrano, S. M., Beguería, S. & López-Moreno, J. I. A multiscalar drought index sensitive to global warming: the standardized precipitation evapotranspiration index. *J. Clim.* **23,** 1696–1718 (2010).
25. Piao, S. *et al.* Spatiotemporal patterns of terrestrial carbon cycle during the 20th century. *Glob. Biogeochem. Cycles* **23,** GB4026 (2009).
26. Schwalm, C. R. *et al.* Does terrestrial drought explain global CO_2 flux anomalies induced by El Niño? *Biogeosciences* **8,** 2493–2506 (2011).
27. Dai, A. Increasing drought under global warming in observations and models. *Nature Clim. Change* **3,** 52–58 (2013).
28. Randerson, J. T. Climate science: global warming and tropical carbon. *Nature* **494,** 319–320 (2013).
29. Ballantyne, A. P., Alden, C. B., Miller, J. B., Tans, P. P. & White, J. W. C. Increase in observed net carbon dioxide uptake by land and oceans during the past 50 years. *Nature* **488,** 70–72 (2012).
30. Graven, H. D. *et al.* Enhanced seasonal exchange of CO_2 by northern ecosystems since 1960. *Science* **341,** 1085–1089 (2013).

Acknowledgements We thank S. Seneviratne and G. Zhang for comments and J. Gash for English editing. This study was supported by the National Natural Science Foundation of China (41125004), the National Basic Research Program of China (grant nos 2010CB950601 and 2013CB956303) and the National Youth Top-notch Talent Support Program in China. R.B.M. was funded by the NASA Earth Science Division.

Author Contributions S. Piao, P. Ciais and X.W. designed the research; X.W. performed the analysis; S. Piao, P. Ciais and X.W. drafted the paper; and P.F., R.B.M., P. Cox., M.H., J.M., S. Peng, T.W., H.Y. and A.C. contributed to the interpretation of the results and to the text.

Author Information Reprints and permissions information is available at www.nature.com/reprints. The authors declare no competing financial interests. Readers are welcome to comment on the online version of the paper. Correspondence and requests for materials should be addressed to S. Piao (slpiao@pku.edu.cn).

METHODS

Atmospheric CO_2 concentration. The measurements of monthly mean atmospheric CO_2 concentration at the Mauna Loa Observatory were obtained from the US National Oceanic and Atmospheric Administration for the period 1959 to 2011 (http://www.esrl.noaa.gov/gmd/ccgg/trends/) and that from the South Pole station were obtained from the Scripps Institution of Oceanography (http://scrippsco2.ucsd.edu/)[31]. Note that about 15% of monthly CO_2 concentrations in the South Pole station during 1959–2011, particularly during the 1960s, were gap-filled (see http://scrippsco2.ucsd.edu for more processing details).

Gridded climate fields. Gridded climate fields used in this study include mean annual temperature (MAT), precipitation, solar radiation, PDSI and SPEI.

Gridded MAT, annual precipitation data and cloud fraction data are from Climatic Research Unit, University of East Anglia[16] (CRU TS 3.2). CRU TS 3.2 provides monthly air temperature, precipitation and other climate variables with spatial resolution of $0.5^\circ \times 0.5^\circ$ over the global land surface during the period 1901–2011. Because solar radiation is not included in the CRU TS 3.2 data set, we used cloud fraction as a surrogate for variations in solar radiation. We further obtained solar radiation from the CRU-NCEP data product (http://dods.extra.cea.fr/store/p529viov/cruncep/). CRU-NCEP is a gridded climate data product combining CRU TS 3.1 and NCEP-NCAR reanalysis. It provides 6-hourly meteorological forcing fields, including solar radiation, for carbon cycle model simulations (see, for example, ref. 2). Given that the discontinuity of the assimilated observations possibly causes the spurious trends in the reanalysis data set[32], the monthly mean value of incoming solar radiation from the NCEP-NCAR reanalysis was corrected in CRU-NCEP to match the empirically derived monthly solar radiation using an approach based on latitude and sunshine hours[33], which was estimated to be proportional to observed cloud fraction in CRU TS 3.1. The preparation of the CRU-NCEP data set was performed in a carbon cycle model intercomparison project[2]. Among all the climate stations used in generating this data set, about 500 are located between 23° north and 23° south, but their spatiotemporal distribution is uneven[16]. For example, ground measurements are particularly sparse over uninhabited area, including the Amazon basin and the tropical rainforest area in Southeast Asia. Thus, we have also used other climate data streams, including different interpolation approaches, climate reanalysis and a combination of ground and satellite measurements, to test the robustness of the inferred increase in γ^{int}_{CGR} to uncertainties in the climate fields. The alternative climate data sets include air temperature fields of the Global Historical Climate Network Gridded Product (GHCN v3) of the National Climatic Data Center[19], which has a spatial resolution of $5^\circ \times 5^\circ$; precipitation fields from the Global Precipitation Climatology Centre[20] (GPCC), which have a spatial resolution of $1^\circ \times 1^\circ$; and a solar radiation data set with a spatial resolution of $1^\circ \times 1^\circ$ (ref. 21). The short-wave radiation product from ref. 21 was obtained by correcting radiation in NCEP-NCAR reanalysis product with satellite-derived SRB v3.0 radiation data[34]. All the data streams (ground measurement interpolation, climate reanalysis, and combination of ground and satellite measurements) have advantages and disadvantages, and thus could have differences despite the general consistency[35,36]. For example, from the late 1990s onwards the CRU data set seems to be giving higher estimates of global precipitation than does GPCC[37]. These differences in the climate data are one of the major sources of uncertainty in γ^{int}_{CGR} estimates (Fig. 2).

The PDSI is a widely used index of drought stress and aridity change[27,38]. We used global PDSI data provided by University Corporation for Atmospheric Research[24]. The PDSI data have a spatial resolution of $2.5^\circ \times 2.5^\circ$ and a temporal resolution of one month from 1850 to 2010. This PDSI data set calculates potential evapotranspiration using the Penman–Monteith equation, which gives more realistic estimates than do Thornthwaite equations[27,37].

The SPEI is a multiscalar drought index similar to the standardized precipitation index but involving a climatic water balance considering both precipitation and evapotranspiration[24]. The timescale of SPEI (or the standardized precipitation index) is defined so that an n-month scale considers the water surplus or deficit accumulated over $n-1$ previous months[24]. Previous studies suggest that timescales ranging from 3 to 12 months are best suited to monitoring various drought types[39]. In this study, we adopted the same 6-month scale for SPEI (SPEI6) as in ref. 40, but also performed all calculations with SPEI on timescales of 3 months (SPEI3), 9 months (SPEI9) and 12 months (SPEI12). The global SPEI data set was provided by ref. 41 with a spatial resolution of $0.5^\circ \times 0.5^\circ$ and a temporal resolution of one month from 1901 to 2011.

Carbon fluxes and soil moisture from global ecosystem models. Annual net biome productivity from 1901 to 2008 was simulated by five dynamic global vegetation models (DGVMs) (HyLand (HYL), Lund-Potsdam-Jena (LPJ), ORCHIDEE (ORC), Sheffield-DGVM (SHE) and TRIFFID (TRI)) in the comparison study of ref. 2, and land carbon sink simulations in ref. 22 (http://dgvm.ceh.ac.uk). Because spatially explicit output from ORCHIDEE was not available before 1972 in this data set, results from an updated ORCHIDEE simulation are used. Starting from pre-industrial equilibrium for all ecosystem carbon pools reached after spin-up, all models were forced with CRU-NCEP climate fields and increasing atmospheric CO_2 concentration for the period 1901–2008. It is important to note that the DGVM models produce only land–atmosphere CO_2 fluxes because of changed climate and CO_2; other drivers, such as nitrogen deposition, forest demography changes and land-use change, are not considered. Four DGVM models (HYL, LPJ, SHE and TRI) have a spatial resolution of $3.75^\circ \times 2.5^\circ$, and the updated ORCHIDEE simulation has a spatial resolution of $0.5^\circ \times 0.5^\circ$.

Analyses. The annual CGR of a specific month is calculated as the difference between the CO_2 concentration in that month and in the same month the previous year. Tropical MAT, annual precipitation, annual solar radiation, annual PDSI and annual SPEI were all calculated as the spatial average over all the vegetated land area between 23° north and 23° south. The vegetated land area is defined as all grid points for which the mean annual normalized difference vegetation index during 1982–2006 was larger than 0.1. Normalized difference vegetation index data were obtained from the Global Inventory Monitoring and Modelling Studies group[42].

Interannual variation of CGR was found to be driven by climate variations, particularly by tropical temperature, on the basis of atmospheric CO_2 observations and terrestrial carbon cycle modelling (see, for example, refs 9, 10). This finding is consistent with field observations that tropical forest growth is more closely linked to variations in temperature than to variations in precipitation and solar radiation[43]. To improve our understanding of the climate–CGR relationship, we also applied a convergent cross-mapping method[18] to detect the linkage between CGR and tropical MAT (or other climate variables).

We calculated γ^{int}_{CGR} over a running time window (ranging from 20 to 25 yr) during the study period. Linear trends, estimated by the least-squares method, were removed from the CGR and tropical climate (MAT, annual precipitation, mean annual solar radiation) time series within each time window. Then γ^{int}_{CGR} was calculated as the regression slope of MAT in a multilinear regression of CGR against MAT, annual precipitation and mean annual incoming solar radiation (all variables detrended). Different time-window lengths were tested, up to a maximum length of 25 yr. This avoids data overlapping between the first and the most recent time window. Considering the fact that detrended CGR and MAT anomalies have 1–2-yr autocorrelation (Extended Data Fig. 10), a minimum time-window length was chosen as 20 yr. Note that, even though γ^{int}_{CGR} calculated with shorter time windows, such as 15 yr, could be affected by autocorrelation, our main result—that γ^{int}_{CGR} increased by a factor of two—is robust to changes in the length of the selected time window. We also calculated γ^{int}_{CGR} using a linear mixed model that specifically accounts for temporal autocorrelation with a first-order autocorrelation function[44,45]. The results show that including data autocorrelation in the regression does not change the value of γ^{int}_{CGR} (Extended Data Fig. 10).

The window-by-window change in γ^{int}_{CGR} was fitted using three different methods: the Mann–Kendall test[46], linear regression of γ^{int}_{CGR} against time, and a regime shift model. We noted that the data overlapping in neighbouring time windows result in too few degrees of freedom to test the statistical significance of the trend in γ^{int}_{CGR}. Thus, statistical tests were made to compare γ^{int}_{CGR} for the earliest time window with that for the most recent time window, which are fully independent from each other.

To test whether the shift in γ^{int}_{CGR} during the study period was an artefact of our detrending method for CGR and tropical climate time series (MAT, annual precipitation and mean annual solar radiation), we applied frequency decomposition by singular spectrum analysis (SSA; see, for example, ref. 18) to extract the interannual variability of CGR and climate variables. Here the monthly CGR time series was decomposed into four frequency components: a high-frequency component[47], a seasonal component, an interannual component and a long-term trend component. Thresholds separating the frequency components were set a priori and constrained by the temporal resolution and length of CGR time series. Frequency components with the variability up to 4.5 months were regarded as the high-frequency component, whereas the thresholds separating seasonal, interannual and long-term trend components were respectively set to be 20 and 90 months, which were equally spaced on the logarithm axis of the frequency domain (see ref. 18 for more detailed descriptions of SSA). The interannual component of the climate variables was obtained in the same way. Then a linear regression between interannual components of CGR and those of the climate variables was calculated to estimate γ^{int}_{CGR}.

To estimate uncertainty in γ^{int}_{CGR}, we calculated it in 500 bootstrap analyses[48], for each combination of different data sources (CGR from Mauna Loa or the South Pole, MAT from CRU or from GHCN, precipitation from CRU or from GPCP, solar radiation from CRU-NCEP and ref. 21, and cloud fraction from CRU as a surrogate for solar radiation), different moving-window lengths (20–25 yr) to calculate γ^{int}_{CGR}, and different methods for filtering the long-term increase in CGR with time (linear regression and SSA). The uncertainty of change in γ^{int}_{CGR} was taken from the 72,000,000 sensitivity tests.

To study the linkage between change in γ_{CGR}^{int} and tropical drought, we grouped the 50 years' worth of data into four distinct bins of detrended tropical moisture anomaly (standardized departure (σ) less than -1, between -1 and 0, between 0 and 1, and greater than 1). For each bin of detrended moisture anomaly, we calculated γ_{CGR}^{int}. The detrended soil moisture (SM) index anomaly is defined as the standardized departure from average of detrended SM:

$$\sigma(i) = \frac{\mathrm{SM}(i) - \mathrm{Mean(SM)}}{\mathrm{Std(SM)}}$$

Here SM(i) is the detrended SM for the year i, and Mean(SM) and Std(SM) are the average and standard deviation of the SM during the whole study period, respectively. An alternative of binning tropical moisture anomalies into eight bins on the basis of σ (less than -1.5, between -1.5 and -1, between -1 and -0.5, between -0.5 and 0, between 0 and 0.5, between 0.5 and 1, between 1 and 1.5, and greater than 1.5) did not qualitatively change the result.

To test the robustness of the observed relationship between γ_{CGR}^{int} and anomalies (Fig. 3), we performed a null Monte Carlo experiment. In the Monte Carlo experiment, we randomly generated artificial time series of CGR, MAT, annual precipitation and annual solar radiation following a multivariate normal distribution defined by the mean and covariations of the observed time series during 1960–2011. Because the relationship between CGR and MAT is forced to be stable during the entire period, we expected no change in γ_{CGR}^{int} (Extended Data Fig. 7). The hypothesis to test is whether the covariations between CGR, MAT and precipitation could result in differences in γ_{CGR}^{int} for different bins of detrended precipitation anomalies, as observed in Fig. 3.

Impacts of interannual CO_2 variations on interannual temperature variations. To estimate quantitatively the impacts of year-to-year variations in CO_2 on temperature variations, we followed refs 49, 50 to calculate the radiative forcing of CO_2 from its concentration, and used the climate sensitivity from different models. The transient temperature change due to changing CO_2 concentration is[50]

$$T_{i+1} - T_i = \frac{\alpha}{\log(2)} \log\left(\frac{C_{i+1}}{C_i}\right)$$

where T_i and C_i are the mean annual temperature and atmospheric CO_2 concentration in year i, respectively, and α is the transient temperature change in response to the doubling of CO_2 concentration. The likely range of transient climate sensitivity is $\alpha = 1.0$–$2.5\ ^{\circ}\mathrm{C}$ (ref. 51). Here we used the largest value in this range to estimate the maximum plausible impact of CO_2 greenhouse effect on temperature variations. The result suggests that the impact of CO_2 variations on interannual temperature variations is one order of magnitude smaller than the observed interannual variations in mean annual temperature. It confirms that the impact of the CO_2 greenhouse effect on temperature is not the reason for the observed significant correlation between CGR and temperature.

31. Keeling, C. D. *et al.* in *A History of Atmospheric CO_2 and its effects on Plants, Animals, and Ecosystems* (eds Ehleringer, J. R. *et al.*) 83–113 (Springer, 2005).
32. Kistler, R. *et al.* The NCEP–NCAR 50-year reanalysis: monthly means CD–ROM and documentation. *Bull. Am. Meteorol. Soc.* **82,** 247–267 (2001).
33. Angstrom, A. Solar and terrestrial radiation: report to the international commission for solar research on actinometric investigations of solar and atmospheric radiation. *Q. J. R. Meteorol. Soc.* **50,** 121–126 (1924).
34. Stackhouse, P. *et al.* 12-year surface radiation budget data set. *GEWEX News* **14,** 10–12 (2004).
35. Dinku, T., Connor, S. J., Ceccato, P. & Ropelewski, C. F. Comparison of global gridded precipitation products over a mountainous region of Africa. *Int. J. Climatol.* **28,** 1627–1638 (2008).
36. Solomon, S. *et al.* (eds) *Climate Change 2007: The Physical Science Basis* 241–265 (Cambridge Univ. Press, 2007).
37. Sheffield, J., Wood, E. F. & Roderick, M. L. Little change in global drought over the past 60 years. *Nature* **491,** 435–438 (2012).
38. Seneviratne, S. I. *et al.* Investigating soil moisture-climate interactions in a changing climate: a review. *Earth Sci. Rev.* **99,** 125–161 (2010).
39. Edwards, D. C. *Characteristics of 20th Century Drought in the United States at Multiple Time Scales*. MSc thesis, Colorado State Univ. (1997).
40. Hirschi, M. *et al.* Observational evidence for soil-moisture impact on hot extremes in southeastern Europe. *Nature Geosci.* **4,** 17–21 (2011).
41. Vicente-Serrano, S. M., Beguería, S., López-Moreno, J. I., Angulo, M. & El Kenawy, A. A new global 0.5° gridded dataset (1901–2006) of a multiscalar drought index: comparison with current drought index datasets based on the Palmer drought severity index. *J. Hydrometeorol.* **11,** 1033–1043 (2010).
42. Tucker, C. J. *et al.* An extended AVHRR 8-km NDVI dataset compatible with MODIS and SPOT vegetation NDVI data. *Int. J. Remote Sens.* **26,** 4485–4498 (2005).
43. Clark, D. A., Piper, S. C., Keeling, C. D. & Clark, D. B. Tropical rain forest tree growth and atmospheric carbon dynamics linked to interannual temperature variation during 1984–2000. *Proc. Natl Acad. Sci. USA* **100,** 5852–5857 (2003).
44. van Mantgem, P. J. & Stephenson, N. L. Apparent climatically induced increase of tree mortality rates in a temperate forest. *Ecol. Lett.* **10,** 909–916 (2007).
45. Carnicer, J. *et al.* Widespread crown condition decline, food web disruption, and amplified tree mortality with increased climate change-type drought. *Proc. Natl Acad. Sci. USA* **108,** 1474–1478 (2011).
46. Mann, H. B. Nonparametric tests against trend. *Econometrica* **13,** 245–259 (1945).
47. Mahecha, M. D., Fürst, L. M., Gobron, N. & Lange, H. Identifying multiple spatiotemporal patterns: a refined view on terrestrial photosynthetic activity. *Pattern Recognit. Lett.* **31,** 2309–2317 (2010).
48. Manly, B. *Randomization, Bootstrap and Monte Carlo Methods in Biology* 3rd edn (Chapman & Hall/CRC, 2007).
49. Solomon, S. *et al.* (eds) *Climate Change 2001: The Scientific Basis* 351–358 (Cambridge Univ. Press, 2007).
50. Hansen, J. *et al.* Global climate changes as forecast by Goddard Institute for Space Studies three-dimensional model. *J. Geophys. Res.* **93,** 9341–9364 (1988).
51. Alexander, L. V. *et al.* in *Climate Change 2013: The Physical Science Basis* (eds Stocker, T. F. *et al.*) 1–33 (Cambridge Univ. Press, 2013).

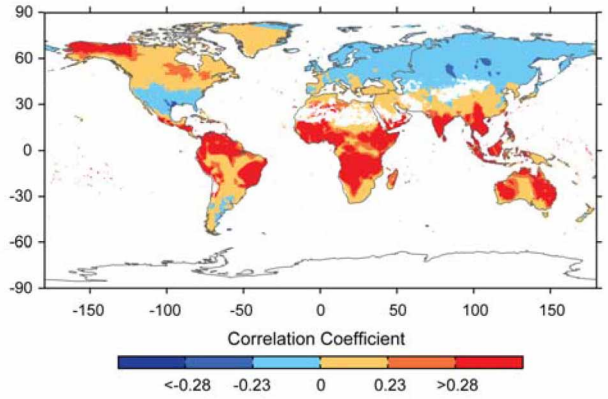

Extended Data Figure 1 | Spatial distribution of the correlation coefficient between detrended CGR and MAT anomalies. CGR anomalies are from Mauna Loa Observatory and local MAT anomalies were derived from the CRU data set for the period 1960–2011. The correlation coefficients 0.23 and 0.28 are the critical thresholds at significance levels of 0.10 and 0.05 ($n = 52$), respectively.

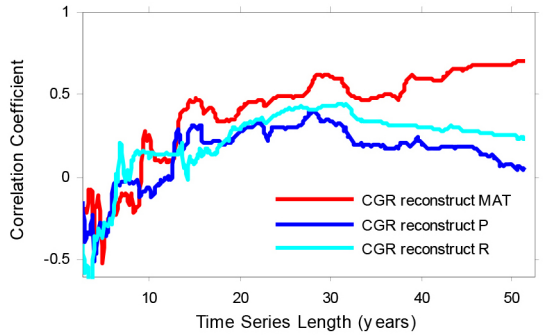

Extended Data Figure 2 | Convergent cross-mapping for reconstruction of variations in MAT, annual precipitation and mean annual solar radiation from variations in CGR. CGR data are from Mauna Loa Observatory. The CGR-reconstructed temperature curve gradually converges to a large positive correlation coefficient ($R = 0.70$), whereas the CGR-reconstructed precipitation (P) and radiation (R) curves lead to smaller correlation coefficients ($R = 0.04$ and $R = 0.23$, respectively) as time-series length increases, suggesting that CGR variations are mainly forced by temperature variations rather than by variations in precipitation and solar radiation.

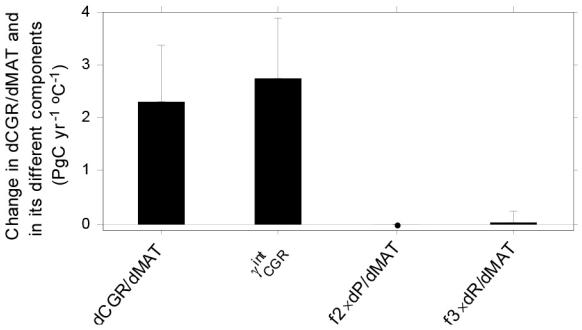

Extended Data Figure 3 | Change in dCGR/dMAT, γ^{int}_{CGR}, and the effects of interannual variations of precipitation and solar radiation on the estimate of dCGR/dMAT. The changes are calculated between the latest two decades and the earliest two decades in 1960–2011. Precipitation and radiation effects are denoted f2 × dP/dMAT and f3 × dR/dMAT, respectively. dCGR/dMAT is calculated as the slope of MAT in the regression of CGR at Mauna Loa Observatory against MAT over the tropical vegetated land. γ^{int}_{CGR}, f2 and f3 are the slopes of MAT, precipitation and radiation, respectively, in the multiple regression of CGR against MAT, precipitation and radiation over the tropical vegetated land. dP/dMAT is the slope of MAT in the regression of precipitation against MAT. dR/dMAT is the slope of MAT in the regression of radiation against MAT. Error bars indicate the 95% confidence interval of the corresponding value derived from 500 bootstrap estimates.

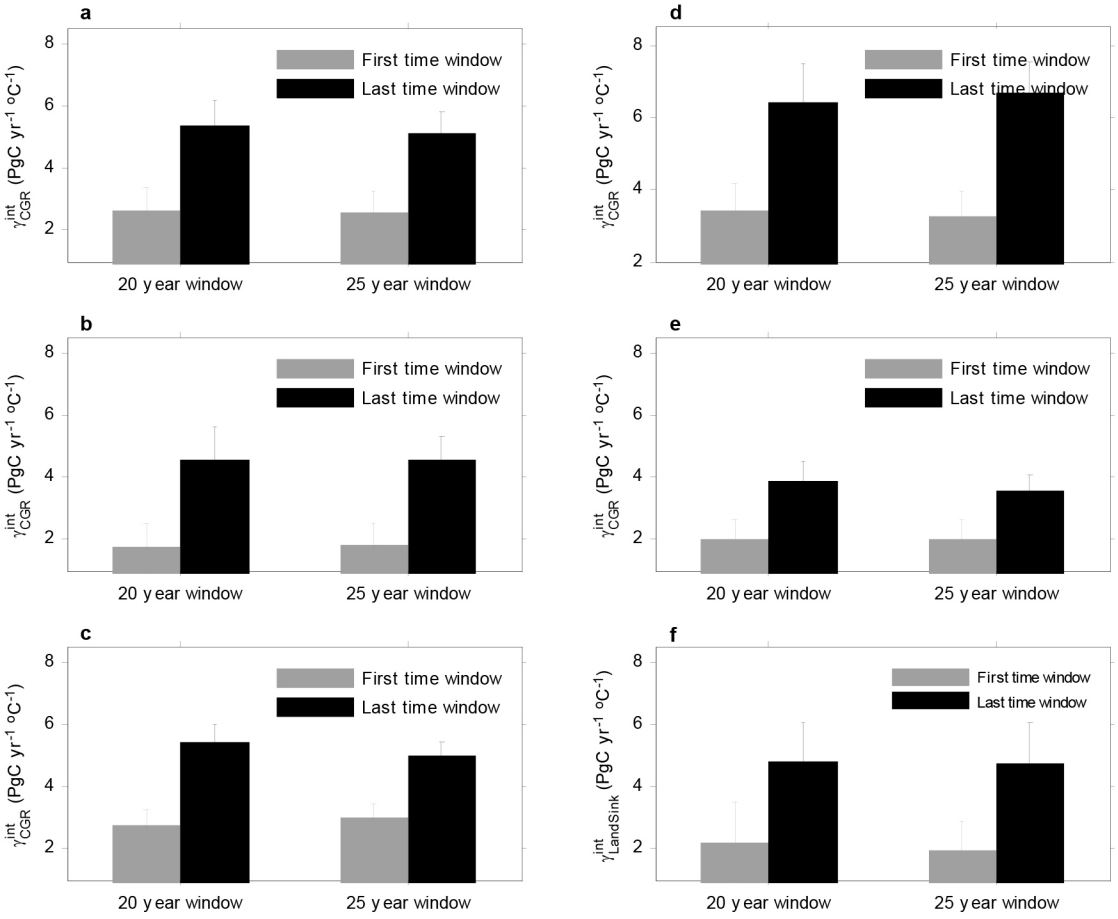

Extended Data Figure 4 | γ^{int}_{CGR} and $\gamma^{int}_{LandSink}$ for the first and the last time window during the study period 1960–2011. For 20-yr windows, the two windows are 1960–1979 and 1992–2011. For 25-yr windows, they are 1960–1984 and 1987–2011. **a**, Data from 1992 and 1993 (post-Pinatubo years) are excluded from γ^{int}_{CGR} estimates. **b**, Data from the record-high El Niño events of 1972–1973 and 1997–1998 are excluded from γ^{int}_{CGR} estimates. **c**, Interannual variations of CGR and climate variables are obtained from the frequency decomposition by SSA (Methods). **d**, γ^{int}_{CGR} is estimated with alternative climate data sets (tropical MAT is from the GHCN data set[19], tropical annual precipitation is from the GPCC[20] and solar radiation is from ref. 21). **e**, CGR is obtained from monthly CO_2 records at the South Pole. **f**, Interannual temperature sensitivity of the residual land carbon sink ($\gamma^{int}_{LandSink}$). The residual land carbon sink of each year is estimated from the CGR by adding the ocean sink and subtracting fossil fuel emission and emission due to land-use change[22]. In **a**–**d**, γ^{int}_{CGR} is estimated from Mauna Loa CO_2 records. Error bars indicate the 95% confidence interval of γ^{int}_{CGR} derived from 500 bootstrap estimates.

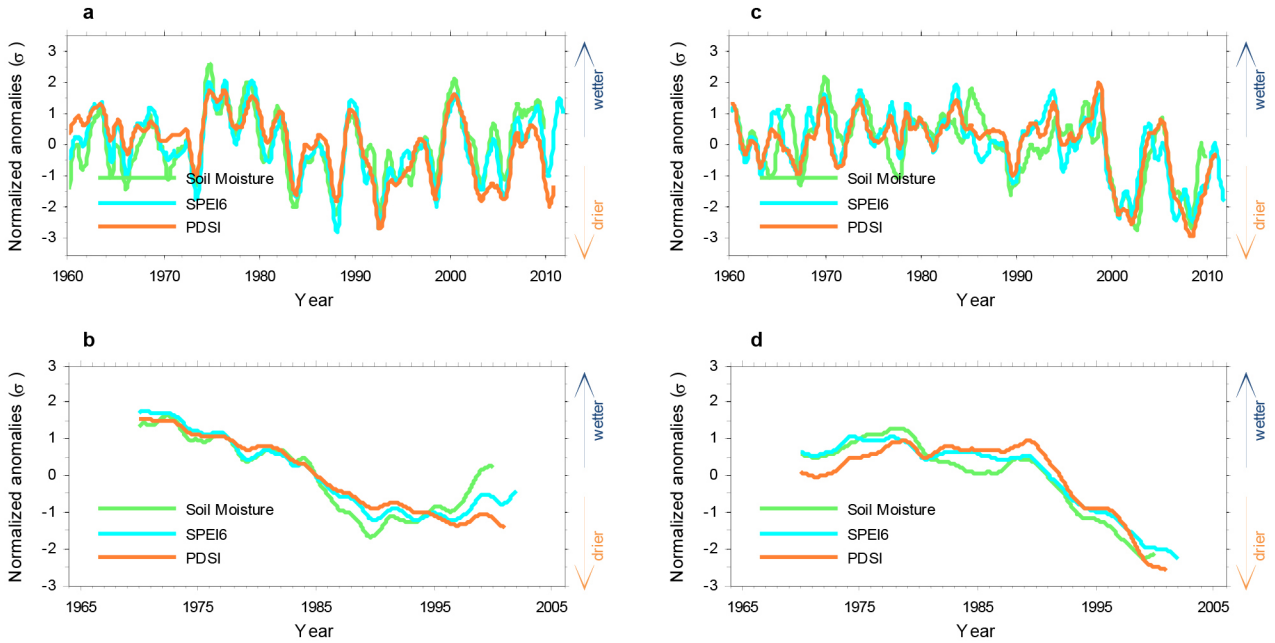

Extended Data Figure 5 | Change in drought indices and 20-yr smoothed drought indices over tropical and mid-latitude regions during the past five decades. **a**, Change in tropical (23° south to 23° north) annual PDSI, SPEI6 and ORCHIDEE-estimated soil moisture. **b**, 20-yr smoothed tropical PDSI, SPEI6 and ORCHIDEE-simulated soil moisture. **c**, Change in mid-latitude (23° north to 48° north) annual PDSI, SPEI6 and ORCHIDEE-simulated soil moisture. **d**, 20-yr smoothed mid-latitude PDSI, SPEI6 and ORCHIDEE-simulated soil moisture. Years on the *x*-axis indicate the central year of the 20-yr time window (for example, 1970 represents 1960–1979). All variables are normalized by their respective standard deviations. The changes in SPEI3, SPEI9 and SPEI12 are close to that in SPEI6. Note that SPEI is available till 2011, PDSI is available till 2010 and model soil moisture is available till 2009.

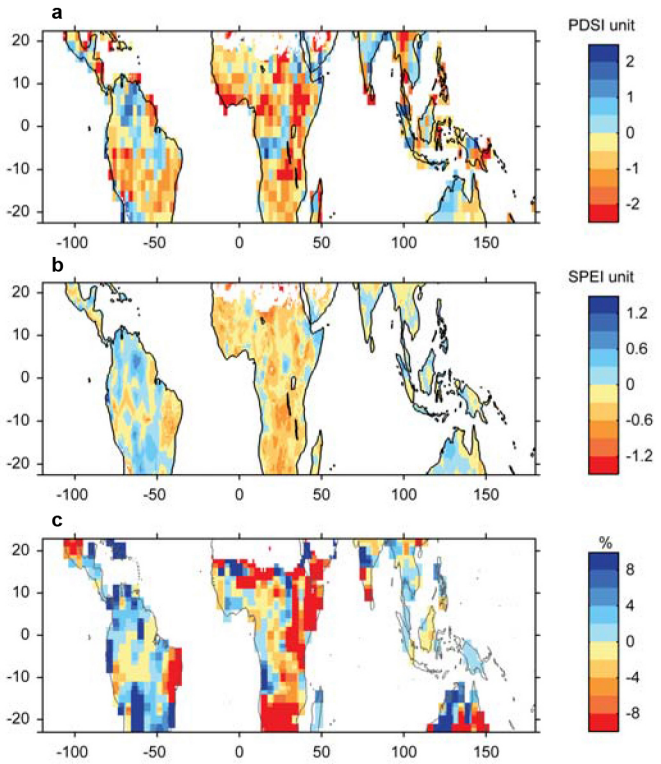

Extended Data Figure 6 | Spatial distribution of the difference between the latest and first 20-yr periods during the past five decades in PDSI, SPEI6 and ORCHIDEE-estimated soil moisture. **a**, PDSI; **b**, SPEI6; **c**, ORCHIDEE-simulated soil moisture. The changes in SPEI3, SPEI9 and SPEI12 are close to that in SPEI6.

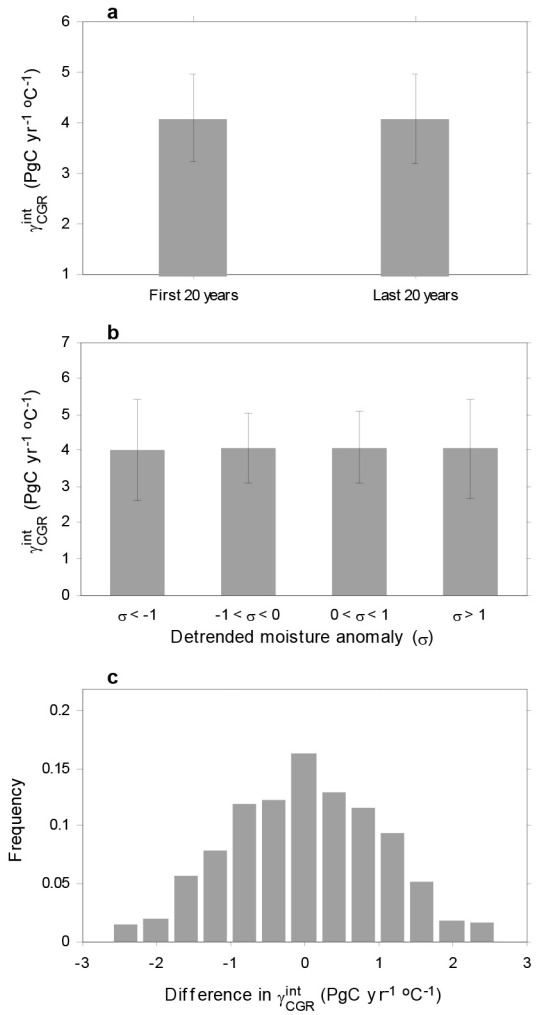

Extended Data Figure 7 | Change in γ^{int}_{CGR} and the relationship between γ^{int}_{CGR} and precipitation anomalies in the null Monte Carlo experiment. **a**, γ^{int}_{CGR} in the first and last 20 yr during 1960–2011. **b**, γ^{int}_{CGR} for each bin of detrended tropical precipitation anomalies, which are divided into four bins (standardized departure (σ) less than -1, between -1 and 0, between 0 and 1, and greater than 1). Values of γ^{int}_{CGR} for different bins of detrended tropical precipitation anomaly are similar. **c**, Frequency distribution of the difference between γ^{int}_{CGR} calculated for $\sigma > 1$ (wet conditions) and γ^{int}_{CGR} calculated for $\sigma < -1$ (dry conditions). The probability of the observed difference (ranging from 5.1 to 6.0 Pg C yr^{-1} °C^{-1}; Fig. 3) occurring purely by chance is very low ($P < 0.01$). Error bars indicate the confidence intervals of the corresponding estimates.

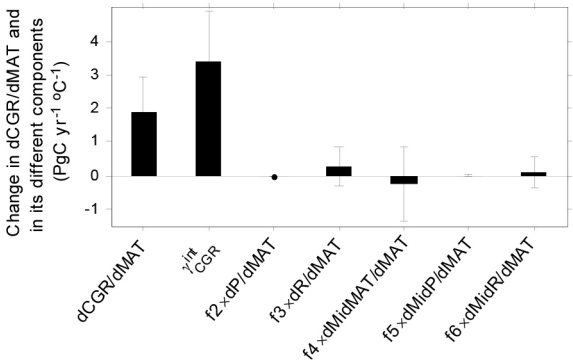

Extended Data Figure 8 | Change in dCGR/dMAT and γ^{int}_{CGR} and variational effects on estimating dCGR/dMAT between the earlier and latest two decades during 1960–2011. The effects of interannual variations of tropical precipitation (P), tropical short-wave solar radiation (R), mid-latitude (23° north to 48° north) temperature (MidMAT), mid-latitude precipitation (MidP) and mid-latitude short-wave solar radiation (MidR) are denoted f2 × dP/dMAT, f3 × dR/dMAT, f4 × dMidMAT/dMAT, f5 × dMidP/dMAT and f6 × dMidR/dMAT, respectively, where f2, f3, f4, f5 and f6 are respectively the slopes of P, R, MidMAT, MidP and MidR in the multiple regression of CGR against P, R, MidMAT, MidP, MidR. dy/dx represents the slope of x in the regression of y against x. Error bars indicate the 95% confidence interval of the corresponding value derived from 500 bootstrap estimates.

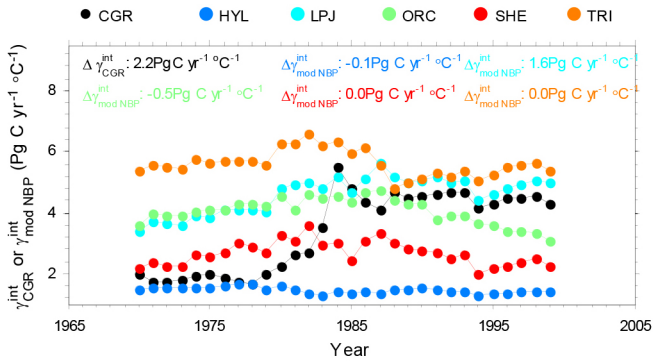

Extended Data Figure 9 | Change in γ^{int}_{CGR} and γ^{int}_{modNBP} during 1960–2008 with a 20-yr moving time window. γ^{int}_{modNBP} is the interannual temperature sensitivity of tropical net biome productivity, estimated using five carbon cycle models (HYL, LPJ, ORC, SHE and TRI). To be consistent with model estimated annual net biome productivity, CGR of a specific year is calculated as the difference between the December Mauna Loa CO_2 concentration of the year and that of December the previous year. Positive value of γ^{int}_{modNBP} indicates reduced anomalies of carbon sinks during warm years.

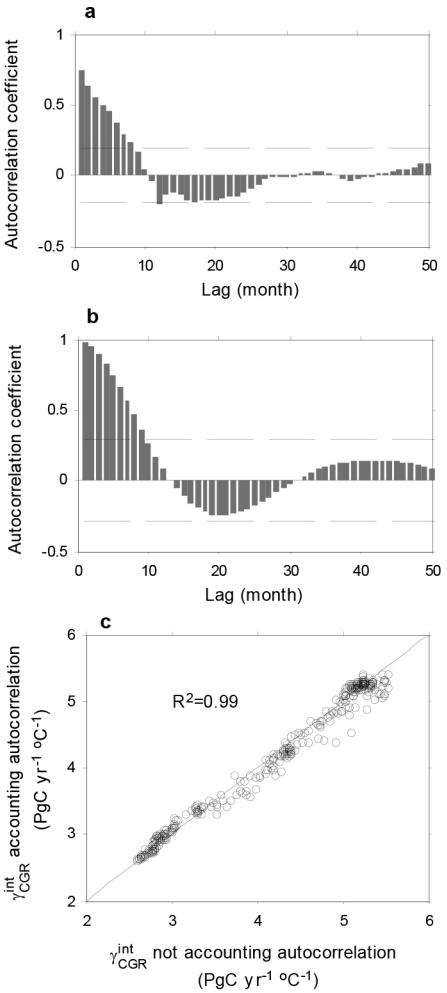

Extended Data Figure 10 | Autocorrelations in CGR and MAT, and their impacts on the estimates of γ^{int}_{CGR}. **a**, Autocorrelation coefficients for detrended anomalies of CGR from Mauna Loa during 1960–2011. **b**, Autocorrelation coefficients for detrended anomalies of MAT during 1960–2011. Dashed lines in **a** and **b** indicate 95% confidence bands. **c**, The comparison between γ^{int}_{CGR} calculated in the multiple regression of interannual variations of the Mauna Loa CGR record against interannual variations in temperature, precipitation and solar radiation (*x* axis) and γ^{int}_{CGR} calculated in the linear mixed model with same independent variables and a first-order autocorrelation function (*y* axis). Solid line indicates 1:1 ratio. This 1:1 relationship holds for γ^{int}_{CGR} derived for different time-window lengths.